Hyperfine structure of the NaK c 3Σ+ state and the effects of perturbation

Kiyoshi Ishikawa, Takahiro Kumauchi, Masaaki Baba, and Hajime Katô

Citation: The Journal of Chemical Physics **96**, 6423 (1992); doi: 10.1063/1.462856
View online: http://dx.doi.org/10.1063/1.462856
View Table of Contents: http://scitation.aip.org/content/aip/journal/jcp/96/9?ver=pdfcov
Published by the AIP Publishing

Hyperfine structure of the NaK $c\,^3\Sigma^+$ state and the effects of perturbation

Kiyoshi Ishikawa, Takahiro Kumauchi, Masaaki Baba,[a] and Hajime Katô
Department of Chemistry, Faculty of Science, Kobe University, Nada-ku, Kobe 657, Japan

(Received 3 December 1991; accepted 28 January 1992)

Scanning the frequency of a single-mode dye laser crossed with a molecular beam of NaK, we have measured the excitation spectrum by monitoring selectively the fluorescence intensity of transition to the $a\,^3\Sigma^+$ state. The $B\,^1\Pi(v=8)$ and $c\,^3\Sigma^+(v=22)$ levels are perturbed around $J=5$ and the $c\,^3\Sigma^+(v=22)$ and $b\,^3\Pi(v\approx 62)$ levels are perturbed around $J=24$. The transition lines to the perturbed levels are fully resolved. The hyperfine splitting, which is induced by the coupling with the nuclear spins of the Na and K atoms, is observed for levels of the $c\,^3\Sigma^+$ state and the perturbed states. The magnitude of the hyperfine splitting, the line intensity, and the energy shift are analyzed, and their relation with the perturbation is studied. The ratio of electron spin densities at the sodium and potassium atoms in the $c\,^3\Sigma^+$ state is estimated to be 0.71:0.15 from the magnitudes of hyperfine splitting.

I. INTRODUCTION

The $B\,^1\Pi$ state of the NaK molecule is strongly perturbed and there has been much interest in studying the perturbation mechanism.[1-7] By scanning the laser frequency and detecting selectively the fluorescence intensity of the transition to the $a\,^3\Sigma^+$ state in a crossed laser–molecular beam arrangement, Kowalczyk *et al.*[3,6] observed the spin-forbidden $c\,^3\Sigma^+$–$X\,^1\Sigma^+$ and $b\,^3\Pi$–$X\,^1\Sigma^+$ transitions. The method is highly sensitive to detect the spin-forbidden transition. The hyperfine splitting is small both in the $X\,^1\Sigma^+$ and $B\,^1\Pi$ states, and no hyperfine structure can be observed in the $B\,^1\Pi$–$X\,^1\Sigma^+$ transition unless the $B\,^1\Pi$ level is perturbed. The hyperfine structure was observed in a transition from the $X\,^1\Sigma^+$ state to a level mixed with the $c\,^3\Sigma^+$ state.[3,5,6] The hyperfine splitting was identified as originating from the Fermi contact interaction between the nuclear moment of ^{23}Na and an electron spin, and the value of hyperfine coupling constant was determined.[6] However, the analysis of the perturbation was not complete because of the lack of accurate molecular constants of the $B\,^1\Pi$ state. Katô *et al.*[7] determined accurate molecular constants of the $B\,^1\Pi$ state by means of the Doppler-free polarization spectroscopy and studied the perturbation between the $B\,^1\Pi$ and $c\,^3\Sigma^+$ states. However, the spin-forbidden transitions could be observed only for strongly perturbed lines by this method.

Crossing a molecular beam of NaK with the beam of a single-mode dye laser and scanning the frequency, we measured the excitation spectrum by monitoring selectively the fluorescence intensity of the transition to the $a\,^3\Sigma^+$ state (see Fig. 1). By this method, we could observe a large number of spin-forbidden transitions with high sensitivity and high resolution. The line broadening due to the hyperfine interaction with the K nucleus could be observed in addition to the hyperfine splitting due to the Na nucleus. We report the results and study the perturbation between the $B\,^1\Pi(v=8)$ and $c\,^3\Sigma^+(v=22)$ levels extensively. The perturbation between the $c\,^3\Sigma^+(v=22)$ and $b\,^3\Pi$ states, which was found by Kowalczyk,[6] is also studied in detail, and Kowalczyk's results are confirmed. The magnitude of the hyperfine splitting, the line intensity, and the energy shift are analyzed, and the relation with the perturbation is studied.

II. EXPERIMENT

The experimental setup is similar to that described in Ref. 8. The molecular beam is produced by expanding the vapor from a 1:2 mixture of sodium and potassium metals at 620 K through a nozzle of 300 μm diameter. The beam contains Na_2, NaK, and K_2 molecules in addition to Na and K

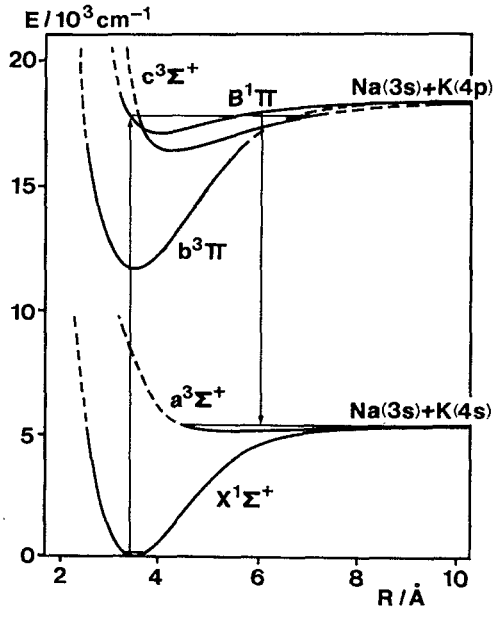

FIG. 1. Potential energy curves of the NaK molecule. The curves of the $X\,^1\Sigma^+$, $a\,^3\Sigma^+$, $b\,^3\Pi$, $c\,^3\Sigma^+$, and $B\,^1\Pi$ states are calculated by the Rydberg–Klein–Rees (RKR) method, respectively, from the molecular constants in Refs. 9, 11, 7, and 20. The excitation spectrum is measured by monitoring selectively the fluorescence to the $a\,^3\Sigma^+$ state.

[a] Present address: College of Liberal Arts and Sciences, Kyoto University, Sakyo-ku, Kyoto 606, Japan.

 0021-9606/92/096423-10$06.00

atoms, but only the NaK molecule absorbs the light in the energy region of the present study. The molecular beam collimated by a skimmer (700 μm diameter, 50 mm from nozzle) is crossed at right angles with the laser light. Scanning the frequency of a single-mode ring dye laser (Coherent CR699-29), we measured the excitation spectrum by monitoring selectively the fluorescence to the $a\,^3\Sigma^+$ state. The selective detection was performed by placing an optical band pass filter, which transmits between 810 and 865 nm, in front of the photomultiplier tube (Hamamatsu 943-02). The resolution of the excitation spectrum is about 20 MHz, due mainly to the residual Doppler width and the natural linewidth. The maximum laser power at the crossing point is kept at less than 5 mW/mm^2 and the absence of any saturation effect was confirmed by measuring the linearity of emission intensity and the independence of the linewidth on the laser power.

III. RESULTS AND DISCUSSION

The excitation spectrum was measured from 17 370 to 17 460 cm^{-1} and part of the spectrum is shown in Fig. 2. In addition to the $B\,^1\Pi(v=8,\ J')$–$X\,^1\Sigma^+(v=0,\ J'')$ transitions, we could observe the transitions to the $c\,^3\Sigma^+(v=22,\ F_1,\ F_2,$ and $F_3)$ levels. These spin-forbidden transitions are allowed through the spin–orbit interaction between the $B\,^1\Pi$ and $c\,^3\Sigma^+$ states, and the strongest perturbation is observed around $J=5$. Hyperfine structures composed of four lines were observed and the magnitude of the hyperfine splitting was observed to change remarkably with J. Some of the hyperfine profiles are shown in Figs. 3 and 4. The hyperfine splittings of the $c\,^3\Sigma^+(v=22,\ F_1)$ and $c\,^3\Sigma^+(v=22,\ F_3)$ levels were observed, respectively, to become small around $N=21$ $(J=22)$ and $N=27$ $(J=26)$. We shall analyze these results quantitatively.

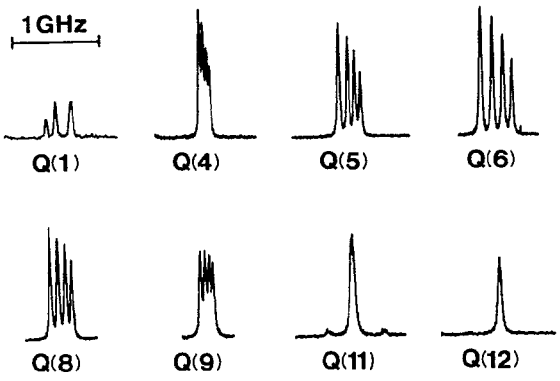

FIG. 3. Observed hyperfine structure of the $B\,^1\Pi(v=8,\ J,\ f)$–$X\,^1\Sigma^+(v=0,\ J)$ transitions $Q(J)$.

A. Analysis of perturbation

The Hamiltonian for a rotating diatomic molecule can be written in the form

$$H_0 = H_e + H_v + H_r + H_{SO}, \tag{1}$$

where H_e is the electronic part, H_v is the vibrational part, H_r is the rotational part, and H_{SO} is the spin–orbit interaction. Wave functions of simple product form $|\Lambda\rangle|S\Sigma\rangle|v\rangle|J\Omega M\rangle$ are used as a set of basis functions. The function $|\Lambda\rangle|S\Sigma\rangle|v\rangle$ is a wave function for a nonrotating molecule, where v is the vibrational quantum number, and Λ and Σ represent, respectively, the projection of the total electronic orbital angular momentum (L) and total electronic spin angular momentum (S) along the molecular axis and are expressed in the molecule-fixed coordinates. The rotational part $|J\Omega M\rangle$ is expressed in the laboratory-fixed coordinates, where the quantum numbers J and M specify, respectively, the total

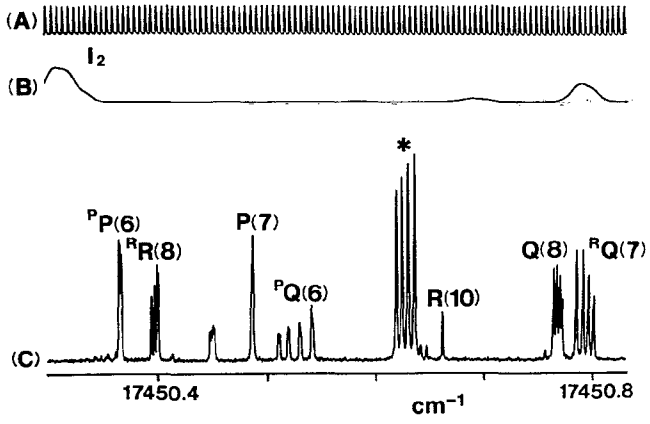

FIG. 2. A part of the Doppler-free excitation spectrum (C). Assignments of the $B\,^1\Pi(v=8,\ J')$–$X\,^1\Sigma^+(v=0,\ J'')$ and $c\,^3\Sigma^+(v=22,\ N,\ J')$–$X\,^1\Sigma^+(v=0, J'')$ transitions are shown above the line. The line marked by * is the $B\,^1\Pi(v=9,\ J=38)$–$X\,^1\Sigma^+(v=0,\ J=38)$ transition. (A) Frequency marks at every 150 MHz of an external Fabry–Perot interferometer. (B) An excitation spectrum of I_2 used to calibrate the wave number.

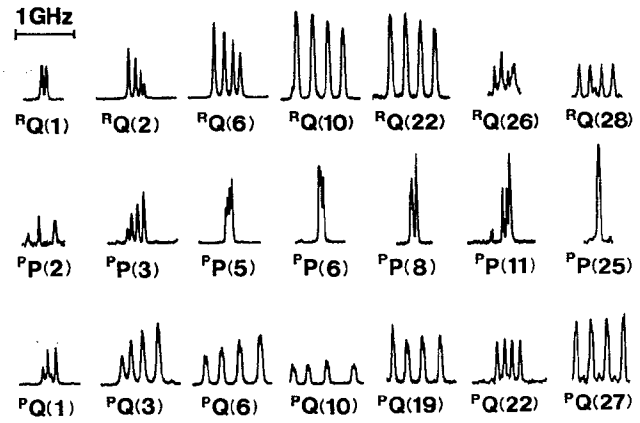

FIG. 4. Observed hyperfine structure of the $c\,^3\Sigma^+(v=22)$–$X\,^1\Sigma^+(v=0)$ transitions. $^RQ(J)$, $^PP(J)$, and $^PQ(J)$ are, respectively, the $c\,^3\Sigma^+(v=22,\ N=J+1,\ F_3)$–$X\,^1\Sigma^+(v=0,\ J)$; $c\,^3\Sigma^+(v=22,\ N=J-1,\ F_2)$–$X\,^1\Sigma^+(v=0,\ J)$; and $c\,^3\Sigma^+(v=22,\ N=J-1,\ F_1)$–$X\,^1\Sigma^+(v=0,\ J)$ transitions.

angular momentum and its projection along the laboratory-fixed Z axis and $\Omega = \Lambda + \Sigma$.

The eigenfunctions for levels of a $^1\Pi$ state [Hund's case (a)] with well-defined parity are

$$|^1\Pi_f^e vJM\rangle = 2^{-1/2}(|1\rangle|00\rangle|v\rangle|J\,1M\rangle \pm |-1\rangle|00\rangle|v\rangle|J-1M\rangle). \quad (2)$$

The eigenvalues are

$$\langle ^1\Pi_f^e vJM\,|H_0|\,^1\Pi_f^e vJM\rangle = E_v + B_v[J(J+1)-1], \quad (3)$$

where E_v is the eigenvalue of $H_e + H_v$ and B_v is the rotational constant of the v level. The eigenfunctions for levels of a $^3\Sigma^+$ state [Hund's case (b)] are

$$|^3\Sigma^+ vN = J+1JM;F_3\rangle = [J/2(2J+1)]^{1/2}(|0^+\rangle|11\rangle|v\rangle|J\,1M\rangle + |0^+\rangle|1-1\rangle|v\rangle|J-1M\rangle) - [(J+1)/(2J+1)]^{1/2}|0^+\rangle|10\rangle|v\rangle|J0M\rangle,$$
$$|^3\Sigma^+ vN = JJM;F_2\rangle = 2^{-1/2}(|0^+\rangle|11\rangle|v\rangle|J\,1M\rangle - |0^+\rangle|1-1\rangle|v\rangle|J-1M\rangle),$$
$$|^3\Sigma^+ vN = J-1JM;F_1\rangle = [(J+1)/2(2J+1)]^{1/2}(|0^+\rangle|11\rangle|v\rangle|J\,1M\rangle + |0^+\rangle|1-1\rangle|v\rangle|J-1M\rangle) + [J/(2J+1)]^{1/2}|0^+\rangle|10\rangle|v\rangle|J0M\rangle, \quad (4)$$

where N is the rotational quantum number. The eigenvalues are

$$\langle ^3\Sigma^+ vNJM\,|H_0|\,^3\Sigma^+ vNJM\rangle = E_v + B_vN(N+1). \quad (5)$$

The eigenfunctions for levels of a $^3\Pi$ state [Hund's case (a)] are

$$|^3\Pi_{0e}^f vJM\rangle = 2^{-1/2}(|1\rangle|1-1\rangle|v\rangle|J0M\rangle \pm |-1\rangle|11\rangle|v\rangle|J0M\rangle),$$
$$|^3\Pi_{1e}^f vJM\rangle = 2^{-1/2}(|1\rangle|10\rangle|v\rangle|J\,1M\rangle \pm |-1\rangle|10\rangle|v\rangle|J-1M\rangle),$$
$$|^3\Pi_{2e}^f vJM\rangle = 2^{-1/2}(|1\rangle|11\rangle|v\rangle|J\,2M\rangle \pm |-1\rangle|1-1\rangle|v\rangle|J-2M\rangle). \quad (6)$$

The eigenvalues are, respectively,

$$\langle ^3\Pi_{0e}^f vJM\,|H_0|\,^3\Pi_{0e}^f vJM\rangle = E_v - A + B_v[J(J+1)+1], \quad \langle ^3\Pi_{1e}^f vJM\,|H_0|\,^3\Pi_{1e}^f vJM\rangle = E_v + B_v[J(J+1)+1],$$
$$\langle ^3\Pi_{2e}^f vJM\,|H_0|\,^3\Pi_{2e}^f vJM\rangle = E_v + A + B_v[J(J+1)-3], \quad (7)$$

where A is the spin–orbit coupling constant. From a simple molecular orbital approximation, the magnitude of A for the NaK $b\,^3\Pi$ state is estimated to be 19.2 cm^{-1}.

The rotational levels $^3\Sigma^+$ (v, N, $J = N-1$, N, and $N+1$) are split by the spin–rotation interaction H_{SR} and the spin–spin interaction H_{SS}. The nonvanishing matrix elements for the wave functions of Eq. (4) are

$$\langle ^3\Sigma^+ vN = J+1JM\,|H_{SR}+H_{SS}|\,^3\Sigma^+ vN = J+1JM\rangle = -(J+2)\gamma_v - \frac{J+2}{2J+1}(2/3)\lambda_v,$$
$$\langle ^3\Sigma^+ vN = JJM\,|H_{SR}+H_{SS}|\,^3\Sigma^+ vN = JJM\rangle = -\gamma_v + (2/3)\lambda_v,$$
$$\langle ^3\Sigma^+ vN = J-1JM\,|H_{SR}+H_{SS}|\,^3\Sigma^+ vN = J-1JM\rangle = (J-1)\gamma_v - \frac{J-1}{2J+1}(2/3)\lambda_v,$$
$$\langle ^3\Sigma^+ vN = J+1JM\,|H_{SR}+H_{SS}|\,^3\Sigma^+ vN = J-1JM\rangle = \frac{3[J(J+1)]^{1/2}}{2J+1}(2/3)\lambda_v, \quad (8)$$

where γ_v and λ_v are, respectively, v-dependent constants of the effective coefficients of the spin–rotation interaction and the spin–spin interaction.

The perturbation between $^1\Pi$ and $^3\Sigma^+$ states is induced by the spin–orbit interaction H_{SO}. The nonvanishing matrix elements of H_{SO} between the wave functions of Eqs. (2) and (4) are

$$\langle ^3\Sigma^+ vN = J+1JM\,|H_{SO}|\,^1\Pi fv'JM\rangle = [J/(2J+1)]^{1/2}\xi_{vv'}, \quad \langle ^3\Sigma^+ vN = JJM\,|H_{SO}|\,^1\Pi ev'JM\rangle = \xi_{vv'},$$
$$\langle ^3\Sigma^+ vN = J-1JM\,|H_{SO}|\,^1\Pi fv'JM\rangle = [(J+1)/(2J+1)]^{1/2}\xi_{vv'}, \quad (9)$$

where $\xi_{vv'}$ is the spin–orbit coupling constant between $^3\Sigma^+$ (v) and $^1\Pi$ (v') levels.

The rotational levels $c\,^3\Sigma^+$ ($v = 22$, $N \leqslant 10$) were found to be perturbed by the $B\,^1\Pi$ ($v = 8$, $J \leqslant 10$) levels and the perturbation was analyzed in detail.[7] We find that the difference between the deperturbed term energies of the $B\,^1\Pi$ ($v = 8$, $J = J'$) and $c\,^3\Sigma^+$ ($v = 22$, $N = J'$) levels increases as J' increases (see Fig. 5). The line intensity of the $c\,^3\Sigma^+$ ($v = 22$, $N > 10$)–$X\,^1\Sigma^+$ ($v = 0$, J'') transition is observed to decrease gradually as N increases and the intensity of the $B\,^1\Pi$ ($v = 8$, $J' > 10$)–$X\,^1\Sigma^+$ ($v = 0$, J'') transition is observed to increase as J' increases. The magnitude of

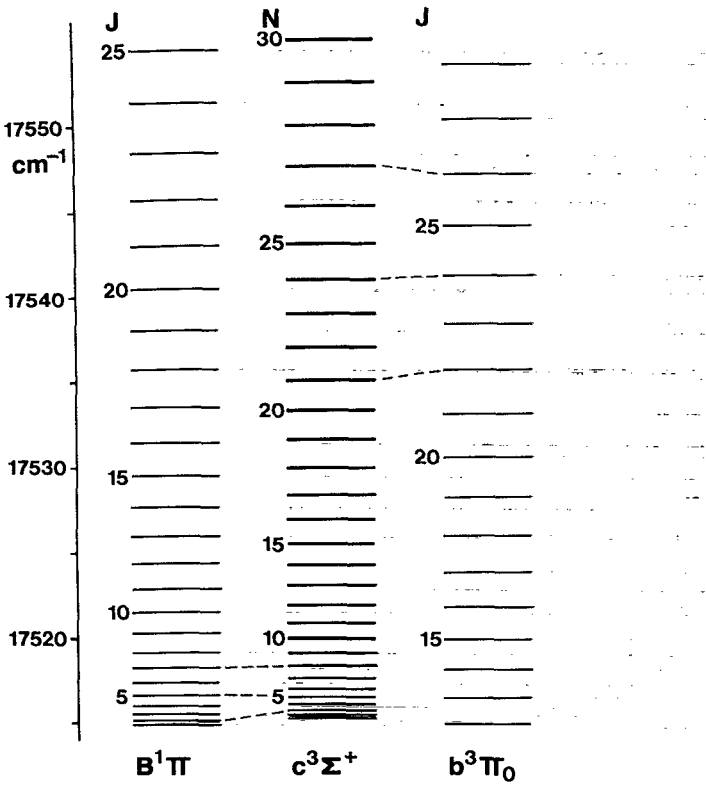

FIG. 5. Deperturbed term energies of the $B\,^1\Pi(v=8, J)$, $c\,^3\Sigma^+(v=22, N)$, and $b\,^3\Pi_0(v_0\approx 62, J)$ levels, which are calculated from the molecular constants in Table I. The strongly perturbing levels are connected by a dashed line.

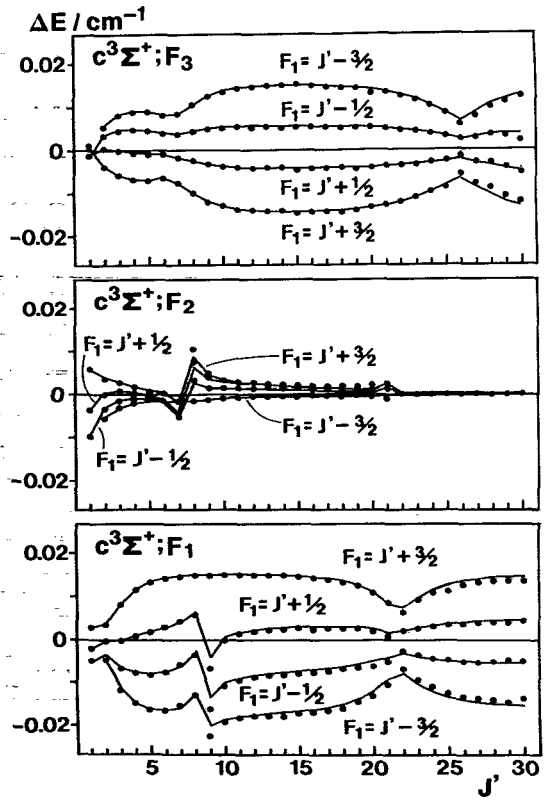

FIG. 6. Observed hyperfine splittings of the $c\,^3\Sigma^+(v=22, N=J'+1, F_3)$; $c\,^3\Sigma^+(v=22, N=J', F_2)$; and $c\,^3\Sigma^+(v=22, N=J'-1, F_1)$ levels are plotted as a function of J' (dots). The line position of each hyperfine component obtained by diagonalizing the matrix of $H_0+H_{SR}+H_{SS}+H_{JL}+H_{FC}$ for all perturbing states, whose molecular constants are listed in Table I, is shown by a line. The origin is the line position calculated by neglecting the hyperfine interaction H_{FC}.

the hyperfine splitting of the $c\,^3\Sigma^+(v=22, N>11)$–$X\,^1\Sigma^+(v=0, J'')$ transition changes abnormally around $N=21$ ($J'=22$) and $N=27$ ($J'=26$) (see Fig. 6). The difference between the observed transition energy and the energy computed from the molecular constants in Refs. 7 and 9 is found to increase as N increases for $N>10$. These facts suggest that the $c\,^3\Sigma^+$ state is perturbed by a state other than the $B\,^1\Pi$ state. The possible perturbing state is the $b\,^3\Pi$ state as we can expect from the potential curves.[10]

The perturbation between $^3\Sigma^+$ and $^3\Pi$ states can occur through the spin–orbit interaction H_{SO} and the L-uncoupling interaction $H_{JL}=-B(J_+L_-+J_-L_+)$, where $J_\pm=J_x\pm iJ_y$, $L_\pm=L_x\pm iL_y$, the suffixes x and y denoting the components of the molecule-fixed coordinates; the z axis is along the internuclear axis. $B=h^2/8\pi^2\mu R^2$, where h is the Planck constant, μ is the reduced mass, and R is the internuclear distance. The nonvanishing matrix elements of H_{SO} between the wave functions of Eqs. (4) and (6) are given by

$$\langle {}^3\Sigma^+ vN=J+1JM|H_{SO}|{}^3\Pi_1 fv'JM\rangle=[J/(2J+1)]^{1/2}\xi'_{vv'},$$
$$\langle {}^3\Sigma^+ vN=J-1JM|H_{SO}|{}^3\Pi_1 fv'JM\rangle=[(J+1)/(2J+1)]^{1/2}\xi'_{vv'},\quad \langle {}^3\Sigma^+ vN=JJM|H_{SO}|{}^3\Pi_1 ev'JM\rangle=\xi'_{vv'},$$
$$\langle {}^3\Sigma^+ vN=J+1JM|H_{SO}|{}^3\Pi_0 fv'JM\rangle=-[2(J+1)/(2J+1)]^{1/2}\xi'_{vv'},$$
$$\langle {}^3\Sigma^+ vN=J-1JM|H_{SO}|{}^3\Pi_0 fv'JM\rangle=[2J/(2J+1)]^{1/2}\xi'_{vv'}. \tag{10}$$

The nonvanishing matrix elements of H_{JL} between the wave functions of Eqs. (4) and (6) are given by

$$\langle {}^3\Sigma^+ vN=J+1JM|H_{JL}|{}^3\Pi_0 fv'JM\rangle=-J\left(\frac{J+1}{2J+1}\right)^{1/2}\langle v|B|v'\rangle\langle 0^+|L_-|1\rangle,$$
$$\langle {}^3\Sigma^+ vN=JJM|H_{JL}|{}^3\Pi_0 ev'JM\rangle=[J(J+1)]^{1/2}\langle v|B|v'\rangle\langle 0^+|L_-|1\rangle,$$

$$\langle {}^3\Sigma^+ vN=J-1JM|H_{JL}|{}^3\Pi_0 fv'JM\rangle = -(J+1)\left(\frac{J}{2J+1}\right)^{1/2}\langle v|B|v'\rangle\langle 0^+|L_-|1\rangle,$$

$$\langle {}^3\Sigma^+ vN=J+1JM|H_{JL}|{}^3\Pi_1 fv'JM\rangle = (J+1)\left(\frac{2J}{2J+1}\right)^{1/2}\langle v|B|v'\rangle\langle 0^+|L_-|1\rangle,$$

$$\langle {}^3\Sigma^+ vN=J-1JM|H_{JL}|{}^3\Pi_1 fv'JM\rangle = -J\left[\frac{2(J+1)}{2J+1}\right]^{1/2}\langle v|B|v'\rangle\langle 0^+|L_-|1\rangle,$$

$$\langle {}^3\Sigma^+ vN=J+1JM|H_{JL}|{}^3\Pi_2 fv'JM\rangle = -\left\{\frac{J[J(J+1)-2]}{2J+1}\right\}^{1/2}\langle v|B|v'\rangle\langle 0^+|L_-|1\rangle,$$

$$\langle {}^3\Sigma^+ vN=JJM|H_{JL}|{}^3\Pi_2 ev'JM\rangle = -[J(J+1)-2]^{1/2}\langle v|B|v'\rangle\langle 0^+|L_-|1\rangle,$$

$$\langle {}^3\Sigma^+ vN=J-1JM|H_{JL}|{}^3\Pi_2 fv'JM\rangle = -\left\{\frac{(J+1)[J(J+1)-2]}{2J+1}\right\}^{1/2}\langle v|B|v'\rangle\langle 0^+|L_-|1\rangle. \quad (11)$$

We found that the $c\,^3\Sigma^+(v=22,\ N=15$–$30,\ F_1,\ F_2$, and $F_3)$ levels were perturbed and the transitions to the perturbed $b\,^3\Pi(v_0,\ J'=15$–$30)$ levels were identified. The value of v_0 could not be identified, but it was estimated to be about 62 from the molecular constants of the $b\,^3\Pi$ state.[11] By neglecting the hyperfine splitting (approximating the line center by the middle of the hyperfine lines), we have determined the tentative molecular constants of the $c\,^3\Sigma^+(v=22)$ and $b\,^3\Pi$ states by a nonlinear least-squares fitting, where the matrix elements of $H_0+H_{SR}+H_{SS}+H_{JL}$ were numerically diagonalized and the molecular parameters were determined so as to reproduce the observed energies. More accurate molecular constants will be obtained by including the effects of the hyperfine interaction in the next section.

The difference between the observed and the interpolated line positions (calculated from the molecular constants in Table I and Ref. 9) is plotted in Fig. 7. The maximum energy difference, which is the one of the $c\,^3\Sigma^+(v=22, N=24, F_2)$ level, is found to be 2.0 cm^{-1}. This means that the matrix element of the interaction between the perturbing states is larger than 2.0 cm^{-1}. If the perturbation between the $c\,^3\Sigma^+(v=22,\ N=24,\ F_2)$ and $b\,^3\Pi(v_0,\ J=24)$ levels is assumed to be originating only from the spin–orbit interaction, then the energy shifts of the $c\,^3\Sigma^+(v=22,\ N=10$–$20)$ levels are calculated to be larger than the observed shifts. On the other hand, if the perturbation is assumed to be originating from the L-uncoupling interaction between the $c\,^3\Sigma^+(v=22,\ N=24,\ F_2)$ and $b\,^3\Pi(v_0,\ J=24)$ levels, then the energy shifts of the $c\,^3\Sigma^+(v=22,\ N=0$–$30)$ levels are calculated to be in good agreement with the experimental results. This is because the matrix element of H_{JL} increases with J [see Eq. (11)], but the matrix element of H_{SO} is independent of J [see Eq. (10)].

Because all of the $c\,^3\Sigma^+(v=22, N=10$–$30, F_1, F_2$, and $F_3)$ levels are observed to be perturbed, the perturbing state is either $^3\Pi_0$ or $^3\Pi_2$ as we can see from Eq. (11). The maximum energy shift of the $c\,^3\Sigma^+(v=22,\ F_1)$ level is found to be smaller than that of the $c\,^3\Sigma^+(v=22,\ F_3)$ level (see Fig. 7). This can be explained by considering the contribution of the spin–orbit interaction. The signs of the matrix elements $\langle {}^3\Sigma^+ vN=J-1JM|H_{SO}|{}^3\Pi_0 fv'JM\rangle$ and $\langle {}^3\Sigma^+ vN=J+1JM|H_{SO}|{}^3\Pi_0 fv'JM\rangle$ are different, but those of the L-uncoupling interaction are the same. Therefore, the values of $\langle {}^3\Sigma^+ vN=J-1JM|H_{JL}+H_{SO}|{}^3\Pi_0 fv'JM\rangle$ and $\langle {}^3\Sigma^+ vN=J+1JM|H_{JL}+H_{SO}|{}^3\Pi_0 fv'JM\rangle$ can be different. On the other hand, there is no nonvanishing matrix element of H_{SO} between $^3\Pi_2$ and $^3\Sigma^+$ states.

We conclude, therefore, that the state perturbing the $c\,^3\Sigma^+(v=22)$ state is the $b\,^3\Pi_0(v_0)$ state and that the perturbation is mainly originating from the L-uncoupling inter-

TABLE I. Molecular constants and interaction coefficients of the $B\,^1\Pi(v=8)$, $c\,^3\Sigma^+(v=22)$, and $b\,^3\Pi_0(v_0)$ states. All values are in units of cm^{-1}.

	$B\,^1\Pi(v=8)$	$c\,^3\Sigma^+(v=22)$	$b\,^3\Pi_0(v_0)$
E_v	17 514.896 0	17 515.300	17 505.72
B_v	$6.128\,3\times10^{-2}$	4.306×10^{-2}	5.933×10^{-2}
D_v	$4.156\,2\times10^{-7}$	2.15×10^{-7}	
γ_v		3.30×10^{-3}	
λ_v		1.33×10^{-1}	
K_1		1.05×10^{-2}	
K_2		6×10^{-4}	
$\xi_{vv'}$	3.989×10^{-1}	1.25×10^{-1}	
$\langle v\|B\|v'\rangle\langle 0^+\|L_-\|1\rangle$		8.37×10^{-2}	

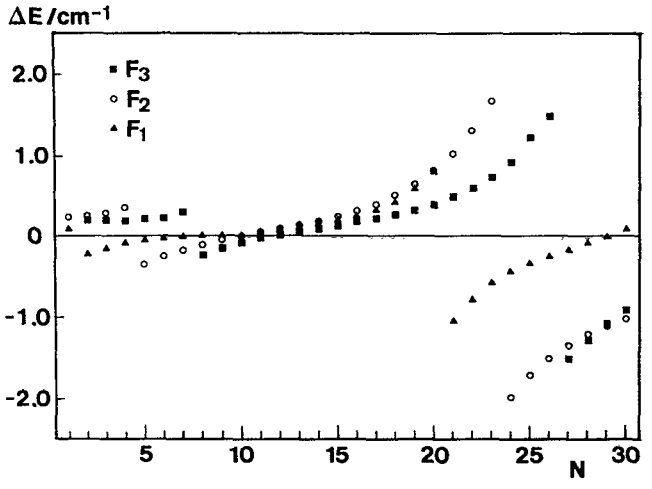

FIG. 7. Deviation of the observed term energies of the $c\,^3\Sigma^+(v=22, N, F_3)$ (■), $c\,^3\Sigma^+(v=22, N, F_2)$ (○), and $c\,^3\Sigma^+(v=22, N, F_1)$ (▲) levels from the energies calculated from the molecular constants of the $c\,^3\Sigma^+(v=22)$ state in Table I and of the $X\,^1\Sigma^+$ state in Ref. 9.

action although the effects of the spin–orbit interaction are not negligible. The magnitudes of the interaction constants $\langle v=22|B|v_0\rangle\langle 0^+|L_-|1\rangle$ and ξ'_{vv_0}, which are determined by the least-squares fitting of level energies, are listed in Table I. The magnitude of the spin–orbit interaction is about 10% of the L-uncoupling interaction around $J=20$.

B. Analysis of hyperfine structures

Hyperfine structures were observed for transitions to the strongly perturbed $B\,^1\Pi$ levels and the $c\,^3\Sigma^+$–$X\,^1\Sigma^+$ transition. The hyperfine splitting was identified[5,6] as originating from the hyperfine splitting of the $c\,^3\Sigma^+$ state induced by the Fermi contact interaction between the ^{23}Na nuclear moment and the electron spin. The total angular momentum $\mathbf{F}_1$ is expressed as $\mathbf{F}_1=\mathbf{J}+\mathbf{I}_1$, where $\mathbf{J}$ is the total angular momentum excluding the nuclear spin angular momentum $\mathbf{I}_1$ of nucleus 1. Let us denote the basis function including the nuclear spin by $|\Lambda S\Sigma v J I_1 F_1 M_{F_1}\rangle$, where M_{F_1} specifies the component of $\mathbf{F}_1$ along the laboratory-fixed Z axis.

For the Fermi contact interaction of nucleus 1 $H_{\rm FC}(1)$, the nonvanishing matrix elements are given by[12–16]

$$\begin{aligned}\langle \Lambda S\Sigma v J I_1 F_1 M_{F_1}|H_{\rm FC}(1)|\Lambda' S'\Sigma' v' J' I_1 F_1' M_{F_1}'\rangle &= \delta_{F_1F_1'}\delta_{M_{F_1}M_{F_1}'}\delta_{\Lambda\Lambda'}\delta_{\Sigma-q\Sigma'}(-)^{J'+I_1+F_1}\begin{Bmatrix} J & J' & 1\\ I_1 & I_1 & F_1\end{Bmatrix}[(2J+1)(2I_1+1)I_1(I_1+1)]^{1/2}(-)^{J+S-\Lambda}\\ &\times[(2S+1)(2J'+1)]^{1/2}\begin{pmatrix} S' & S & 1\\ \Sigma-q & -\Sigma & q\end{pmatrix}\\ &\times\begin{pmatrix} J' & J & 1\\ \Lambda+\Sigma-q & -\Lambda-\Sigma & q\end{pmatrix}(8\pi/3)\zeta(1)\langle \Lambda S v\|\sum_i \mathbf{s}_i(i)\delta(r_{i1})\|\Lambda S' v'\rangle,\end{aligned}\tag{12}$$

where $\langle\|\ \|\rangle$ represents the reduced matrix element, r_{i1} is the distance between electron i and nucleus 1, and $\zeta(1)=gg_1\mu_B\mu_N$. g, g_1, μ_B, and μ_N are, respectively, the g value for an electron, the g value for the nucleus 1, the Bohr magneton, and the nuclear magneton. The nonvanishing matrix elements for the $^3\Sigma^+$ state are

$$\langle {}^3\Sigma^+ vN=J+1JI_1F_1M_{F_1}|H_{\rm FC}|{}^3\Sigma^+ vN=J+1JI_1F_1M_{F_1}\rangle = K_1(F_1JI_1)\left[\frac{1}{(J+1)(2J+1)}-\frac{2}{2J+1}\right],\tag{13}$$

$$\langle {}^3\Sigma^+ vN=JJI_1F_1M_{F_1}|H_{\rm FC}|{}^3\Sigma^+ vN=JJI_1F_1M_{F_1}\rangle = K_1(F_1JI_1)/J(J+1),\tag{14}$$

$$\langle {}^3\Sigma^+ vN=J-1JI_1F_1M_{F_1}|H_{\rm FC}|{}^3\Sigma^+ vN=J-1JI_1F_1M_{F_1}\rangle = K_1(F_1JI_1)\left[\frac{1}{J(2J+1)}+\frac{2}{2J+1}\right],\tag{15}$$

$$\begin{aligned}\langle {}^3\Sigma^+ vN=JJI_1F_1M_{F_1}|H_{\rm FC}|{}^3\Sigma^+ vN=JJ-1I_1F_1M_{F_1}\rangle = &-K_1\frac{1}{2J}\left(\frac{J+1}{2J+1}\right)^{1/2}[(F_1+J+I_1+1)(J+I_1-F_1)\\ &\times(F_1+J-I_1)(F_1+I_1+1-J)]^{1/2},\end{aligned}\tag{16}$$

$$\begin{aligned}\langle {}^3\Sigma^+ vN=JJI_1F_1M_{F_1}|H_{\rm FC}|{}^3\Sigma^+ vN=JJ+1I_1F_1M_{F_1}\rangle = &-K_1\frac{1}{2(J+1)}\left(\frac{J}{2J+1}\right)^{1/2}[(F_1+J+I_1+2)\\ &\times(J+I_1+1-F_1)(F_1+J+1-I_1)(F_1+I_1-J)]^{1/2},\end{aligned}\tag{17}$$

where

$$(FJI)=[F(F+1)-J(J+1)-I(I+1)]/2,\tag{18}$$

$$K_1=(8\pi/3)\zeta(1)\langle 01v\|\sum_i \mathbf{s}_1(i)\delta(r_{i1})\|01v\rangle/2^{1/2},\tag{19}$$

$I_1=3/2$ for ^{23}Na, and hence, F_1 takes the values of $J+3/2$, $J+1/2$, $J-1/2$, and $J-3/2$. Equation (14) and the first terms of Eqs. (13) and (15) arise from the $\Delta\Sigma=0$ interaction. The second terms of Eqs. (13) and (15) arise from the $\Delta\Sigma=\pm 1$ interaction. The second terms are dominant for

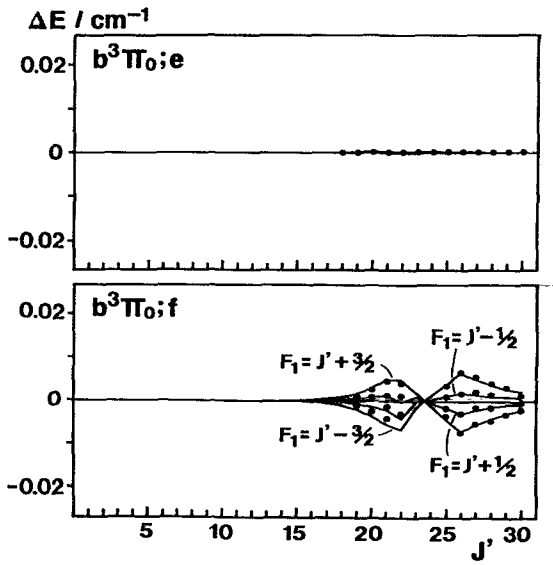

FIG. 8. Observed hyperfine splittings of the $b\,^3\Pi_0$ (v_0, J', e and f) levels are plotted as a function of J' (dots). The line position of each hyperfine component obtained by diagonalizing the matrix of $H_0 + H_{SR} + H_{SS} + H_{JL} + H_{FC}$ for all perturbing states, whose molecular constants are listed in Table I, is shown by a line. The origin is the line position calculated by neglecting the hyperfine interaction H_{FC}.

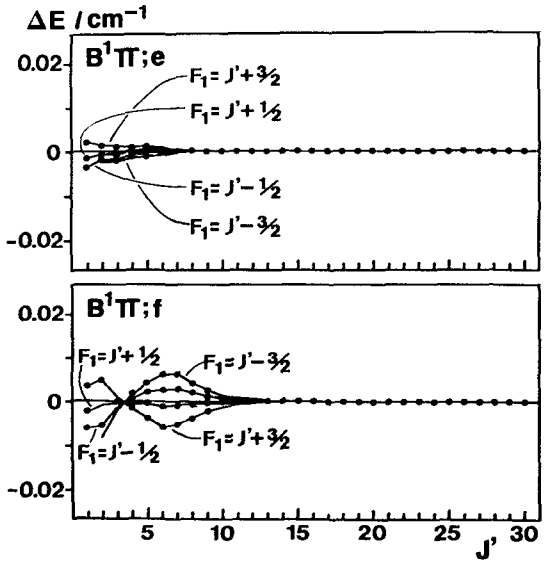

FIG. 9. Observed hyperfine splittings of the $B\,^1\Pi(v = 8,\ J',\ e$ and $f)$ levels are plotted as a function of J' (dots). The missing dots are not resolved because of overlapping with other lines. The line position of each hyperfine component obtained by diagonalizing the matrix of $H_0 + H_{SR} + H_{SS} + H_{JL} + H_{FC}$ for all perturbing states, whose molecular constants are listed in Table I, is shown by a line. The origin is the line position calculated by neglecting the hyperfine interaction H_{FC}.

large J. The hyperfine splitting of the $b\,^3\Pi_0$–$X\,^1\Sigma^+$ transition is observed to be much smaller than that of the $c\,^3\Sigma^+$–$X\,^1\Sigma^+$ transition unless it is strongly perturbed (see Figs. 6 and 8). Therefore, we considered the hyperfine splitting of the $b\,^3\Pi_0$ state to be negligible. This is a good approximation for a $^3\Pi_0$ state in Hund's case (a) because the diagonal matrix element of H_{FC} is zero for a $^3\Pi_0$ state.[17]

The matrix of the Hamiltonian $H_0 + H_{SR} + H_{SS} + H_{JL} + H_{FC}$ for wave functions $|B\,^1\Pi\ v = 8, J, f$ and $e\rangle$, $|c\,^3\Sigma^+ v = 22, N, F_1, F_2$, and $F_3\rangle$, and $|b\,^3\Pi_0\ v_0, f$ and $e\rangle$ was numerically diagonalized and the molecular constants were determined by a nonlinear least-squares fit so as to reproduce the observed energies of all lines including the hyperfine splitting. The resulting molecular constants are listed in Table I. The fits with the observed values are very good and the results are shown in Figs. 6, 8, and 9.

In the region of strong perturbation between the $B\,^1\Pi$ and $c\,^3\Sigma^+$ states, each rotational level of the $B\,^1\Pi$ state is observed to split into the hyperfine components. The $B\,^1\Pi(v = 8,\ J,\ f)$ level interacts strongly with the $c\,^3\Sigma^+(v = 22,\ N,\ F_1)$ level at $J < 3$. At $J < 3$, the $B\,^1\Pi(v = 8,\ J,\ f)$ levels split into the hyperfine components and the splittings of the $c\,^3\Sigma^+(v = 22,\ N,\ F_1)$ levels decrease (Figs. 6 and 9). At $J = 4$–9, the $B\,^1\Pi(v = 8,\ J,\ f)$ level interacts strongly with the $c\,^3\Sigma^+(v = 22,\ N,\ F_3)$ level. The $B\,^1\Pi(v = 8,\ J = 4$–$9,\ f)$ levels split into hyperfine components and the splittings of the $c\,^3\Sigma^+(v = 22,\ N,\ F_3)$ levels become small at $N = 4$–9. The order of the hyperfine components $F_1 = J + 3/2, J + 1/2, J - 1/2$, and $J - 3/2$ of the $B\,^1\Pi(v = 8,\ J = 4$–$9,\ f)$ levels is opposite to that of $J < 3$ and this is due to the fact that the $B\,^1\Pi(v = 8,\ J,\ f)$ level is mixed with the $c\,^3\Sigma^+(v = 22,\ N,\ F_1)$ level at $J < 3$ and with the $c\,^3\Sigma^+(v = 22,\ N,\ F_3)$ level at $J = 4$–9. For the $c\,^3\Sigma^+$ state, the order of the hyperfine components $F_1 = J + 3/2, J + 1/2, J - 1/2$, and $J - 3/2$ agrees with the order expected from the vector model.[17]

An abnormal hyperfine structure and energy shift are observed for transitions to the $c\,^3\Sigma^+(v = 22,\ N = 6$–$11,\ F_2)$ and $c\,^3\Sigma^+(v = 22,\ N = 6$–$11,\ F_1)$ levels. It is identified as originating from the $\Delta N = 0$ and $\Delta J = \pm 1$ hyperfine interaction, whose matrix elements are given by Eqs. (16) and (17). For example, the energy separation between the $c\,^3\Sigma^+(v = 22,\ N = 8,\ J = 8)$ and $c\,^3\Sigma^+(v = 22, N = 8,\ J = 9)$ levels is very small in the absence of the hyperfine interaction and the two levels are strongly mixed by the hyperfine interaction.

The hyperfine splittings of the $c\,^3\Sigma^+(v = 22,\ N,\ F_1)$ and $c\,^3\Sigma^+(v = 22,\ N,\ F_3)$ levels decrease, respectively, around $N = 21$ $(J = 22)$ and $N = 27$ $(J = 26)$. Correspondingly, the hyperfine splitting of the $b\,^3\Pi_0(v_0,\ J,\ f)$ level is observed around $J = 22$ and 26. The hyperfine components $F_1 = J + 3/2, J + 1/2, J - 1/2$, and $J - 3/2$ of the $b\,^3\Pi_0(v_0,\ J = 15$–$23,\ f)$ levels are in reverse order to those of the $b\,^3\Pi_0(v_0,\ J = 25$–$30,\ f)$ levels. This is because the $b\,^3\Pi_0(v_0,\ J,\ f)$ level is mixed with the $c\,^3\Sigma^+(v = 22,\ N,\ F_1)$ level at $J = 15$–23 and with $c\,^3\Sigma^+(v = 22,\ N,\ F_3)$ at $J = 25$–30.

Let us now discuss the line intensity of the hyperfine structure. We measured the excitation spectrum by monitor-

ing selectively the fluorescence to the $a\,^3\Sigma^+$ state. The strong lines with hyperfine structure are observed for strongly perturbed lines. The hyperfine splitting originates from the $c\,^3\Sigma^+$ state and the magnitude of the hyperfine splitting depends on the mixing ratio of the $c\,^3\Sigma^+$ state. The eigenfunction of the perturbed level $B\,^1\Pi(v=8,\ J<10)$ is a mixture of the wave functions $|B\,^1\Pi vJF_1\rangle$ and $|c\,^3\Sigma^+ vNJF_1\rangle$. The line intensity of the excitation spectrum for each hyperfine component $B\,^1\Pi(v,\ J,\ F_1)$–$X\,^1\Sigma^+(v'',\ J'',\ F_1'')$ is proportional to

$$(C_S)^2(C_T)^2 \sum_{M_{F_1}} \sum_{M'_{F_1}} |\langle B\,^1\Pi vJF_1M_{F_1}| \times \mu | X\,^1\Sigma^+ v''J''F_1''M''_{F_1}\rangle|^2, \tag{20}$$

where $(C_S)^2$ is the square of the coefficient of $|B\,^1\Pi vJF_1\rangle$ and $(C_T)^2$ is a sum of squares of the coefficients of $|c\,^3\Sigma^+ vNJF_1\rangle$ ($N=J+1, J$, and $J-1$) in the eigenfunction of a perturbed $B\,^1\Pi(v,\ J,\ F_1)$ level. The matrix element of the laboratory-fixed R_λ component of an electric dipole moment between hyperfine components is given by

$$\langle \Lambda S\Sigma vJI_1F_1M_{F_1}|\mu_{R_\lambda}|\Lambda'S'\Sigma'v'J'I_1F_1'M'_{F_1}\rangle = \delta_{SS'}\delta_{\Sigma\Sigma'}(-)^{-I_1+M'_{F_1}-\Lambda'-\Sigma'}[(2F_1+1)(2F_1'+1)(2J+1)(2J'+1)]^{1/2}\begin{pmatrix} F_1 & 1 & F_1' \\ M_{F_1} & -\lambda & -M'_{F_1}\end{pmatrix} \times \begin{Bmatrix} F_1 & F_1' & 1 \\ J' & J & I_1\end{Bmatrix} \sum_t (-)^{\lambda-t}\langle \Lambda v|\mu_{r_t}|\Lambda'v'\rangle \begin{pmatrix} J & J' & 1 \\ \Lambda+\Sigma & -\Lambda'-\Sigma' & -t\end{pmatrix}, \tag{21}$$

where μ_{r_t} is the molecule-fixed r_t component of an electric dipole moment.

We calculated the line intensity for each hyperfine component and simulated the hyperfine spectrum by using the eigenfunctions and eigenvalues, which were obtained above by diagonalizing the matrix of $H_0+H_{SR}+H_{SS}+H_{JL}+H_{FC}$. The simulated spectra of the $c\,^3\Sigma^+(v=22,\ N,\ F_1$ and $F_3)$–$X\,^1\Sigma^+(v=0,\ J)$ transition are shown in Fig. 10. The agreement with the observed spectra shown in Fig. 4 is very good. When the $\Delta N=0$ and $\Delta J=\pm 1$ hyperfine interaction is negligible, the intensities of four hyperfine components $F_1=J+3/2,\ J+1/2,\ J-1/2$, and $J-3/2$ are proportional to the degeneracy $2F_1+1$ on M_{F_1}. For the $c\,^3\Sigma^+(v=22,\ N,\ F_3)$ level, the $J-3/2$ component appears at higher energy than the $J+3/2$ component as we can see from Eq. (13). It is opposite for the $c\,^3\Sigma^+(v=22,\ N,\ F_1)$ level as we can see from Eq. (15). When the perturbation is strong, the value of $(C_S)^2(C_T)^2$ for each hyperfine component can be different from others because the energy spacings between the perturbing hyperfine levels can be different. The transition to a strongly perturbed level shows a strong line intensity. This is in accordance with the magnitude of $(C_S)^2(C_T)^2$, which is large if the perturbation is strong.

By using approximate wave functions expressed by a single configuration $|0\rangle|10\rangle = (2)^{-1/2}[|(\sigma s)(\overline{\sigma p_0})| + |(\overline{\sigma s})(\sigma p_0)|]$ and $|0\rangle|11\rangle = |(\sigma s)(\sigma p_0)|$, where $|\cdots|$ represents a normalized determinant, ( ) and $\overline{(\ )}$ represent, respectively, molecular orbitals (MOs) with α and β spin, we have

$$\langle 0|\langle 10|\langle v|\sum_i s_{1-1}(i)\delta(r_{i1})|0\rangle|11\rangle|v\rangle = (2)^{-1}[\langle \sigma s(i)|\delta(r_{i1})|\sigma s(i)\rangle + \langle \sigma p_0(i)|\delta(r_{i1})|\sigma p_0(i)\rangle]. \tag{22}$$

Using the Wigner–Eckart theorem, we have

$$\langle 0|\langle 10|\langle v|\sum_i s_{1-1}(i)\delta(r_{i1})|0\rangle|11\rangle|v\rangle = (2)^{-1/2}\langle 01v\|\sum_i \mathbf{s}_1(i)\delta(r_{i1})\|01v\rangle. \tag{23}$$

From Eqs. (19), (22), and (23), we obtain

$$K_1 = (8\pi/3)\zeta(1)[\langle \sigma s(i)|\delta(r_{i1})|\sigma s(i)\rangle + \langle \sigma p_0(i)|\delta(r_{i1})|\sigma p_0(i)\rangle]/2. \tag{24}$$

By assuming primitive linear-combination-of-atomic orbital (LCAO) MOs $|\sigma s\rangle = a|3s^{Na}\rangle + b|4s^K\rangle$ and

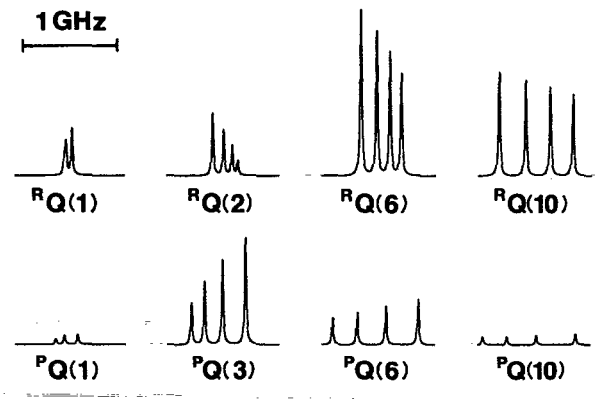

FIG. 10. Simulated hyperfine spectra of the $c\,^3\Sigma^+(v=22, N=J+1, F_3)$–$X\,^1\Sigma^+(v=0,\ J)$ transition $[^RQ(J)]$ and the $c\,^3\Sigma^+(v=22,\ N=J-1,\ F_1)$–$X\,^1\Sigma^+(v=0,\ J)$ transition $[^PQ(J)]$. The relative line intensity and energy separation are calculated from the eigenfunctions and eigenvalues obtained by diagonalizing the matrix of $H_0+H_{SR}+H_{SS}+H_{JL}+H_{FC}$ for all perturbing states, whose molecular constants are listed in Table I. The linewidth (fullwidth at half-maximum) of each hyperfine component is assumed to be 20 MHz.

$|\sigma p_0\rangle = c|3p_z^{Na}\rangle + d\,|4p_z^K\rangle$, where $|\chi^n\rangle$ represents χ^n atomic orbitals of nucleus n, and a, b, c, and d are the coefficients, we have

$$K_1 = (8\pi/3)\zeta(1)\,[a^2\langle 3s^{Na}|\delta(r_1)|3s^{Na}\rangle + 2ab\,\langle 3s^{Na}|\delta(r_1)|4s^K\rangle + b^2\langle 4s^K|\delta(r_1)|4s^K\rangle + c^2\langle 3p_z^{Na}|\delta(r_1)|3p_z^{Na}\rangle + 2cd\,\langle 3p_z^{Na}|\delta(r_1)|4p_z^K\rangle + d^2\langle 4p_z^K|\delta(r_1)|4p_z^K\rangle\,]/2. \quad (25)$$

The hyperfine constant of the $c\,^3\Sigma^+$ state induced by the Fermi contact interaction between the ^{23}Na nuclear moment and the electron spin is then expressed by neglecting small terms as

$$K_{Na}(c\,^3\Sigma^+) = (8\pi/3)\zeta(\mathrm{Na})a^2\langle 3s^{Na}|\delta(r_{Na})|3s^{Na}\rangle/2. \quad (26)$$

The hyperfine structure of the Na($3s\,^2S_{1/2}$) atom arises from the Fermi contact interaction and the value of $K_{Na}(3s\,^2S_{1/2}) = (8\pi/3)\zeta(\mathrm{Na})\langle 3s^{Na}|\delta(r_{Na})|3s^{Na}\rangle$ is reported to be 2.95×10^{-2} cm^{-1}.[18] From the observed hyperfine splitting, we determined the value of $K_{Na}(c\,^3\Sigma^+)$ to be 1.05×10^{-2} cm^{-1}. Therefore, the coefficient a is evaluated to be 0.84.

An expanded spectrum of the $c\,^3\Sigma^+(v'=22,\ N=5,\ F_1)$–$X\,^1\Sigma^+(v''=0, J''=6)$ transition is shown in Fig. 11. The resolution of our excitation spectrum is about 20 MHz and the width of each of the four hyperfine lines is observed to be about 80 MHz. Similar broadening is observed for the lines of large hyperfine splitting (see Fig. 4). The hyperfine structure of the K($4s\,^2S_{1/2}$) atom, which arises from the Fermi contact interaction, has been studied, and the value of $K_K(4s\,^2S_{1/2})$ is reported to be 0.77×10^{-2} cm^{-1}.[18] The

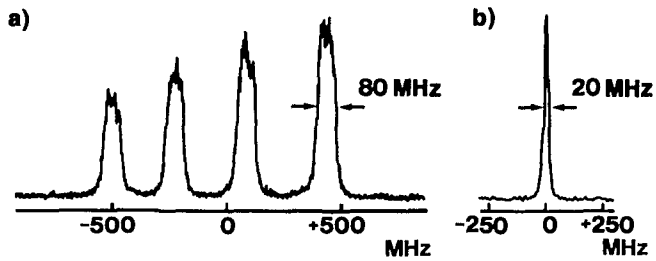

FIG. 11. (a) Observed hyperfine spectrum of the $c\,^3\Sigma^+(v'=22,\ N=5,\ F_1)$–$X\,^1\Sigma^+(v''=0, J''=6)$ transition [$^PQ(6)$]. (b) Observed spectrum of the $c\,^3\Sigma^+(v'=22,\ N=25,\ F_2)$–$X\,^1\Sigma^+(v''=0,\ J''=24)$ transition [$^RR(24)$], which shows that our spectral resolution is 20 MHz.

electric quadrupole interaction of the Na and K atoms is much smaller than the magnetic dipole interaction.[18] Therefore, we ascribe the observed line broadening to the hyperfine splitting of the $c\,^3\Sigma^+$ state induced by the Fermi contact interaction between the ^{39}K nuclear moment and the electron spin.

When two nuclei with nuclear spins $\mathbf{I}_1$ and $\mathbf{I}_2$ have different coupling energies, it is convenient to employ the coupling scheme $\mathbf{J}+\mathbf{I}_1=\mathbf{F}_1$, $\mathbf{F}_1+\mathbf{I}_2=\mathbf{F}_2$, where the nuclear spins are coupled in order of decreasing coupling energy.[16] The basis function for this coupling scheme is denoted by $|\Lambda S\Sigma v J I_1 F_1 I_2 F_2 M_{F_2}\rangle$. The diagonal matrix elements of the Fermi contact interaction for a $^3\Sigma^+$ state are

$$\langle {}^3\Sigma^+ vN=J+1JI_1F_1I_2F_2M_{F_2}|H_{FC}|{}^3\Sigma^+ vN=J+1JI_1F_1I_2F_2M_{F_2}\rangle = K_2\frac{(I_1F_1J)(F_2F_1I_2)}{F_1(F_1+1)(J+1)}, \quad (27)$$

$$\langle {}^3\Sigma^+ vN=JJI_1F_1I_2F_2M_{F_2}|H_{FC}|{}^3\Sigma^+ vN=JJI_1F_1I_2F_2M_{F_2}\rangle = -K_2\frac{(I_1F_1J)(F_2F_1I_2)}{F_1(F_1+1)J(J+1)}, \quad (28)$$

$$\langle {}^3\Sigma^+ vN=J-1JI_1F_1I_2F_2M_{F_2}|H_{FC}|{}^3\Sigma^+ vN=J-1JI_1F_1I_2F_2M_{F_2}\rangle = -K_2\frac{(I_1F_1J)(F_2F_1I_2)}{F_1(F_1+1)J}, \quad (29)$$

where

$$K_2 = (8\pi/3)\zeta(2)\langle 01v\|\Sigma\mathbf{s}_1(i)\delta(r_{i2})\|01v\rangle/2^{1/2}. \quad (30)$$

The reduction of hyperfine splitting due to the mixing of the $B\,^1\Pi$ state is taken into account by using the results of the perturbation analysis and the value of $K_K(c\,^3\Sigma^+)$ is estimated to be 0.06×10^{-2} cm^{-1}. In the same way as we derived Eq. (26), the hyperfine constant of the $c\,^3\Sigma^+$ state induced by the Fermi contact interaction between the ^{39}K nuclear moment and the electron spin is expressed as

$$K_K(c\,^3\Sigma^+) = (8\pi/3)\zeta(\mathrm{K})b^2\langle 4s^K|\delta(r_K)|4s^K\rangle/2. \quad (31)$$

From $K_K(c\,^3\Sigma^+) = 0.06\times10^{-2}$ and $K_K(4s\,^2S_{1/2}) = 0.77\times10^{-2}$ cm^{-1}, the coefficient b is evaluated to be 0.39.

From the normalization condition of $|\sigma s\rangle = a|3s^{Na}\rangle + b\,|4s^K\rangle$, we obtain $a^2+2ab\,\langle 3s^{Na}|4s^K\rangle + b^2 = 1$. For $a=0.84$ and $b=0.39$, we obtain $\langle 3s^{Na}|4s^K\rangle = 0.22$. This is smaller than 0.38, which is the overlap integral for the atomic orbitals (Gaussian 433/4 for $3s^{Na}$, 4333/43 for $4s^K$)[19] at the equilibrium distance 4.258 Å of the $c\,^3\Sigma^+$ state. However, this discrepancy is not significant in due consideration of use of a simple MO approximation. The ratio of $a^2=0.71$:$b^2=0.15$ gives us an approximate ratio of spin densities at the Na and K atoms in the $c\,^3\Sigma^+$ state.

ACKNOWLEDGMENTS

The authors are very grateful to Professor Ch. Ottinger for reading the manuscript and useful comments. This work is supported by a Grant-in-Aid for Scientific Research from the Ministry of Education, Science and Culture.

[1] E. J. Breford, F. Engelke, G. Ennen, and K. H. Meiwes, Faraday Discuss. Chem. Soc. **71**, 233 (1981).
[2] R. F. Barrow, R. M. Clements, J. Derouard, N. Sadeghi, C. Effantin, J. d'Incan, and A. J. Ross, Can. J. Phys. **65**, 1154 (1987).
[3] P. Kowalczyk, B. Krüger, and F. Engelke, Chem. Phys. Lett. **147**, 301 (1988).
[4] J. Derouard and N. Sadeghi, J. Chem. Phys. **88**, 2891 (1988).
[5] M. Baba, S. Tanaka, and H. Katô, J. Chem. Phys. **89**, 7049 (1988).
[6] P. Kowalczyk, J. Chem. Phys. **91**, 2779 (1989).
[7] H. Katô, M. Sakano, N. Yoshie, M. Baba, and K. Ishikawa, J. Chem. Phys. **93**, 2228 (1990).
[8] H. Katô, T. Kobayashi, M. Chosa, T. Nakahori, T. Iida, S. Kasahara, and M. Baba, J. Chem. Phys. **94**, 2600 (1991).
[9] A. J. Ross, C. Effantin, J. d'Incan, and R. F. Barrow, Mol. Phys. **56**, 903 (1985).
[10] W. J. Stevens, D. D. Konowalow, and L. B. Ratcliff, J. Chem. Phys. **80**, 1215 (1984).
[11] A. J. Ross, C. Effantin, J. d'Incan, and R. F. Barrow, J. Phys. B **19**, 1449 (1986).
[12] C. H. Townes and A. L. Schawlow, *Microwave Spectroscopy* (McGraw–Hill, New York, 1955).
[13] R. A. Frosch and H. M. Foley, Phys. Rev. **88**, 1337 (1952).
[14] K. F. Freed, J. Chem. Phys. **45**, 4214 (1966).
[15] M. Broyer, J. Vigué, and J. C. Lehmann, J. Phys. (Paris), **39**, 591 (1978).
[16] R. L. Cook and F. C. De Lucia, Am. J. Phys. **39**, 1433 (1971).
[17] H. Geisen, D. Neuschäfer, and Ch. Ottinger, Z. Phys. D **4**, 263 (1987).
[18] E. Arimondo, M. Inguscio, and P. Violino, Rev. Mod. Phys. **49**, 31 (1977).
[19] *Gaussian Basis Sets for Molecular Calculations*, edited by S. Huzinaga (Elsevier, Amsterdam, 1984).
[20] S. Kasahara, M. Baba, and H. Katô, J. Chem. Phys. **94**, 7713 (1991).